Mon. Not. R. Astron. Soc. **000**, 1–6 (2003) Printed 12 July 2007 (MN LATEX style file v2.2)

Mid-infrared imaging and modelling of the dust shell around post-AGB star HD 187885 (IRAS 19500-1709)

K. L. Clube[1⋆] and T. M. Gledhill[1]
[1]*Dept. of Physics, Astronomy & Maths, University of Hertfordshire, College Lane, Hatfield, UK, AL10 9AB*

12 July 2007

ABSTRACT
We present 10 and 20 μm images of IRAS 19500-1709 taken with the mid-infrared camera, OSCIR, mounted on the Gemini North Telescope. An extended circumstellar envelope is detected, with the N band image indicating an elongation in a NE-SW direction. We use a dust radiation transport code to fit the spectral energy distribution from UV to sub-mm wavelengths, with a detached dust shell model. A good fit is achieved using dust composed of amorphous carbon, silicon carbide and magnesium sulphide. We derive estimates for the inner and outer radius, density and mass of the dust in the shell. The inner radius is not resolved in our OSCIR imaging, giving an upper limit of 0.4 arcsec. With this constraint, we conclude that IRAS 19500-1709 must be at least 4 kpc away in order to have the minimum luminosity consistent with a post-AGB status.

Key words: radiative transfer – stars: AGB and post-AGB – stars: circumstellar matter – stars: mass loss – stars: individual: IRAS 19500-1709 – stars: individual: HD 187885.

1 INTRODUCTION

Post-AGB stars are evolved stars with low to intermediate mass (0.8-8.0 $M_\odot$) progenitors, that have left the Asymptotic Giant Branch (AGB) but not yet become the central stars of Planetary Nebulae (PN) (see review by van Winckel 2003). The heavy mass-loss that occurred on the AGB has ended and the dust envelope that surrounds the star, as a result of this mass-loss, expands away from the star, decreasing in temperature while the temperature of the central star increases. During this relatively short (10^3-10^4 years) phase, these cool dust rich envelopes radiate most of their energy at mid- and far-infrared wavelengths. Observations in the mid-infrared probe the inner, warmest part of the envelope, the area of most recent mass-loss which occurred near the end of the AGB. Studies of individual objects in this transitional post-AGB phase can be used to investigate this final period of AGB mass-loss and to determine the physical and chemical properties of the dust.

IRAS 19500-1709 is associated with the high galactic latitude F2-3I (Parthasarathy, Pottasch & Wamsteker 1988) post-AGB star HD 187885 (SAO 163075) and has the double-peaked spectral energy distribution (SED) typical of post-AGB stars with detached circumstellar dust envelopes (Hrivnak, Kwok & Volk 1989). The radiation from the star, reddened by the dust shell, peaks at around 1 μm whereas the thermal emission, from the shell itself, peaks at 25-30 μm. The post-3rd-dredge-up status of this object is confirmed by its high abundance of s-process elements (van Winckel & Reyniers 2000). The expansion velocity of the envelope, based on the CO-line emission, is 11 km s^{-1} with wings up to 30 km s^{-1} (Likkel et al. 1987). The envelope is carbon rich, showing no OH or H_2O maser emission (Likkel 1989). It has a weak 21 μm feature (Justtanont et al. 1996) and a broad feature around 30 μm (Hony, Waters & Tielens 2002). The origin of these two features is unknown. von Helden et al. (2000) identified titanium carbide (TiC) as the carrier of the 21μm feature but this has recently been disputed by Li (2003). Speck & Hofmeister (2004) have suggested that SiC may carry the 21 μm feature. Goebel & Moseley (1985) proposed that the 30 μm feature may be due to magnesium sulphide (MgS). The central star has a temperature of 8000 K (van Winckel & Reyniers 2000). Imaging polarimetry has shown that IRAS 19500-1709 has a bipolar structure in scattered light (Gledhill et al. 2001).

In section 2 of this paper we present 10 and 20 μm images of IRAS 19500-1709 taken with the mid-infrared camera, OSCIR, on Gemini North[1]. In section 3 we discuss the

⋆ E-mail: kclube@star.herts.ac.uk

[1] Based on observations obtained at the Gemini Observatory, which is operated by the Association of Universities for Research in Astronomy, Inc; under a cooperative agreement with the NSF on behalf of the Gemini partnership:the National Science Foundation (United States), the Particle Physics and Astronomy Re-

results of our modelling of these images and of the SED using a dust radiation transport (RT) code.

2 OBSERVATIONS

We present 10 and 20 μm (N and Q3 band) images of IRAS 19500-1709 taken on 2001 July 12 with OSCIR, mounted on the 8.1-m Gemini North Telescope (Fig. 1). OSCIR is a mid-infrared camera and spectrometer system built by the University of Florida Infrared Astrophysics Group. The array field of view is 11 x 11 arcsec and the pixel scale 0.089 arcsec. We used the standard nodding/chopping mid-infrared observational technique to correct for the thermal background with a chop frequency of 3 Hz and a chop throw of 15 arcsec. For each filter, frame times were 10 ms and on-source exposure times were 4.3 min. For flux calibration we used Vega, which we observed before and after observing IRAS 19500-1709. Atmospheric transmission, as determined by the Vega measurements, varied throughout the night and average calibration factors have been calculated. The resultant N and Q3 band fluxes, obtained by summing over the whole object, are given in Table 1. We have also used the Vega observations as an indication of the point spread function (PSF) and the full width at half-maximum (FWHM) is shown in Table 1 along with other observing details.

Flat-field images were obtained for each filter by exposing on sky and on a polystyrene flat-field source without chopping and nodding and the flat-field constructed using the OFLAT task, which is part of the GEMINI package within IRAF[2]. The observations were reduced using the OREDUCE task in the GEMINI IRAF package which derives the average of the chop and nod differences and produces a single flat-field-corrected image for each filter. A few lines of bad pixels on these images, caused by an OSCIR channel problem which was present during the early Gemini observing runs, were fixed using an IDL procedure provided by Scott Fisher (OSCIR support team).

The images of IRAS 19500-1709 show that it is extended relative to the PSF, with a FWHM of 1.2 arcsec in both filters and diameter of 4 arcsec. The N band image appears elongated in the outer contours with position angle (PA) of 20 ± 10 deg. We note that the telescope PSF, as determined by observations of Vega, is also elongated in a similar direction (shown contoured in Fig. 1). However, the outer contours of the Q3 band image appear round, although the PSF is also elongated, suggesting that the elongation seen in the outer regions of the N band image may be real. This interpretation is strengthened by previous lower spatial resolution imaging which also tentatively suggests an elliptical structure with PA 30 ± 10 deg. (Meixner et al. 1997). The brightness peak in the N band image appears approximately 0.2 arcsec off centre to the east, relative to the outer contours. The inner boundary, of any detached shell, is unresolved.

Table 1. Measurements for IRAS 19500-1709 for each filter showing the central wavelength (λ_c), bandpass ($\Delta\lambda$), flux and the FWHM of the PSF, estimated from observations of Vega. Due to variations in sky transparency, the errors on the fluxes may be as large as $\pm$50 per cent.

Filter	λ_c (μm)	$\Delta\lambda$ (μm)	Flux (Jy)	FWHM (Vega) (arcsec)
N wide	10.75	5.23	33	0.51
Q3	20.80	1.65	134	0.64

3 MODELLING AND DISCUSSION

We use the dust RT code originally developed by Efstathiou & Rowan-Robinson (1990), which solves the radiation transfer equation for an axisymmetric distribution of dust around a central source. The code allows up to seven different grain materials and has been modified to include a power-law size distribution of dust grains (Gledhill & Yates 2003). Although the code is fully 2-D, we use a spherically symmetric dust shell to model 19500-1709 since there is only tentative evidence for axisymmetry in the OSCIR observations and this would not provide sufficient constraints to justify the inclusion of the additional parameters required by a 2-D model.

The input parameters to a spherical shell model include the ratio of the stellar radius to the inner shell radius (r_*/r_1), the ratio of the inner shell radius to the outer shell radius (r_1/r_2), and the stellar temperature ($T_{\rm eff}$). The dust density is specified by the extinction ($A_{\rm v}$) through the shell with the dust density assumed to decline with radius as r^{-2}, corresponding to a constant mass-loss rate. The absorption and scattering efficiencies are calculated for each grain type using Mie theory with the dust properties determined by the optical constants and grain sizes. We assume spherical dust grains with radii between $a_{\rm min}$ and $a_{\rm max}$ with a size distribution of $n(a) \propto a^{-q}$.

The resultant model spectrum is plotted against the observational data for IRAS 19500-1709, which have been taken from the literature. These include optical and near-infrared photometry (Hrivnak et al. 1989), a 7.6-23.6 μm UKIRT spectrum (CGS3) provided by K. Justtanont, *IRAS* fluxes, 8.5, 10 and 12.2 μm flux (Meixner et al. 1997), *IUE* data[3], *ISO* SWS[4] and LWS[5] spectra and JCMT flux (van der Veen et al. 1994).

3.1 Fitting the SED

Around 90 models were run and the best-fitting model, as assessed by eye, is shown in Fig. 2. The final model includes dust composed of amorphous carbon (amC), silicon carbide (SiC) and magnesium sulphide (MgS) grains. The amC dust fits the continuum of the SED quite well.

search Council (United Kingdom), the National Research Council (Canada), CONICYT (Chile), the Australian Research Council (Australia), CNPq (Brazil) and CONICET (Argentina).

[2] Image Reduction and Analysis Facility is distributed by the National Optical Astronomy Observatories, which is operated by the Association of Universities for Research in Astronomy, Inc., under cooperative agreement with the National Science Foundation

[3] Based on INES data from the *IUE* satellite

[4] *ISO* SWS06 observing program rszczerba-PPN30

[5] *ISO* LWS01 observing program mbarlow-dust 3

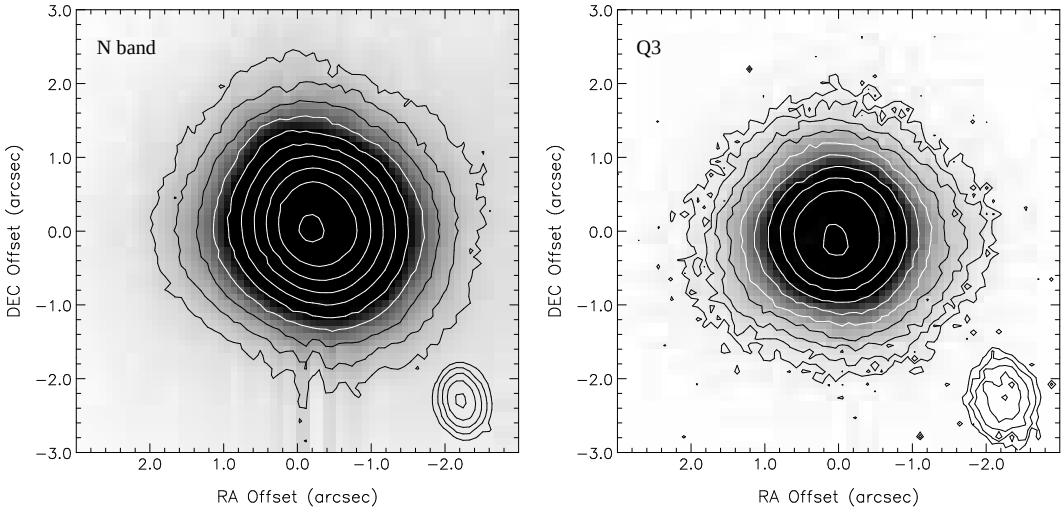

Figure 1. Images of IRAS 19500-1709 from the OSCIR camera on Gemini North using N and Q3 filters. The PSF is shown contoured in the lower right corners. All innermost contours are 95% of the peak values and spaced at 0.5 magnitude increments.

The broad emission feature, extending from 10-13 μm and peaking around 12 μm was observed by Justtanont et al. (1996) but has not been conclusively identified. Although SiC is thought to be a common dust component in carbon stars (Speck et al. 1997), it results in a feature which peaks at 11.3 μm and is too narrow to fit the broad 12 μm 'plateau' feature. However, in the absence of an alternative identification, we have used α-SiC optical constants (Pègouriè 1988) to produce a feature in this wavelength range. The 8-10 μm region is also problematic, in that it exhibits unidentified features. Kwok, Volk & Bernath (2001) suggest that these 8 and 12 μm plateau features may be due to aromatic and aliphatic hydrocarbons. Justtanont et al. (1996) propose that a polycyclic aromatic hydrocarbon (PAH), such as chrysene ($C_{18}H_{12}$), provides the best match to UIR features in the 8-13 μm region. We have briefly explored PAH materials using the cross-sections of Li & Draine (2001) but find that the features produced are too narrow to match the plateau-nature of the observed emission and additional features in the 16-25 μm region of the spectrum are produced, which are not seen in the data.

We include MgS as being the possible carrier of the 30 μm band. It has been found to provide a reasonable fit to this feature (Hony et al. 2002). We used optical constants for $Mg_xFe_{(1-x)}S$ from Begemann et al (1994) with x=0.9, as an approximation to MgS (also see Szczerba et al. 1997, Hony et al. 2003). These data do not extend below 10 μm however, so it was necessary to approximate the optical and UV extinction cross-sections to ensure that the MgS grains absorb sufficient radiation at short wavelengths to radiate in the mid-IR. This was done by adopting the optical constants of parallel graphite (Draine & Lee 1984) below 4 μm and interpolating between 4 and 10 μm to produce a smooth extinction curve. The model shows a feature in the UV part of the spectrum, between 0.2-0.25 μm. Both parallel graphite and amC show structure in their extinction cross sections in this region. The feature around 30 μm is broader and peaks at a longer wavelength than that produced by our model. This may be because we have used spherical grains. Variations in grain shape can influence the emission profile, with ellipsoidal grains producing a broader peak (Hony et al. 2002). Szczerba et al. (1999) suggest that the 30 μm feature may be related to the 21 μm feature, as stars with the 21 μm feature seem to have the 30 μm feature as well. The reverse is not the case though; the 21 μm feature is very weak in 19500-1709, which van Winckel & Reyniers (2000) suggest may be due to the temperature of this object as the feature is observed to be stronger in the cooler 21 μm post-AGB stars in their sample. It certainly seems possible that the 30 μm feature may be due to an unknown carbonaceous component, rather than MgS, as it is a feature which is only seen in carbon rich objects.

In our model the central star is assumed to radiate as a black body with $T_{\rm eff}$ = 8000 K. This temperature is higher than has been previously assumed in some of the literature (e.g. Hrivnak et al. (1989), Gürtler, Kömpe & Henning (1996), Meixner et al. (1997) use temperatures of 7000-7500 K which have been estimated from the spectral type). However detailed analysis of spectral line data suggests a higher temperature of 8000 K (van Winckel & Reyniers (2000)) so we adopt this as the most reliable estimate. Parthasarathy et al. (1988) suggested a temperature of 8500 K might be required to fit the UV spectrum of IRAS 19500-1709 which they found to be peculiar because of a broad absorption feature around 0.17 μm. Increasing the temperature of the central star improves the fit around the UV part of the SED but also increases the prominence of the SiC emission feature. So an increase in temperature needs to be balanced with a decrease in the abundance of SiC. However if the abundance of amC is too high the model does not fit the data around 15-25 μm. A dust mixture comprising 40 per cent amC, 30 per cent SiC and 30 per cent MgS provided the best fit to the data.

A value of $A_{\rm v}$=1.2 provided the best fit around the UV and optical part of the spectrum. Increasing $A_{\rm v}$ results in too much extinction in this region and also too much mid-IR flux. Larger dust grains produce too much flux in the UV and optical region and too strong an emission feature around 11 μm but insufficient flux in the mid-IR peak. A value of $a_{\rm min}$=0.01 μm yielded the best results along with

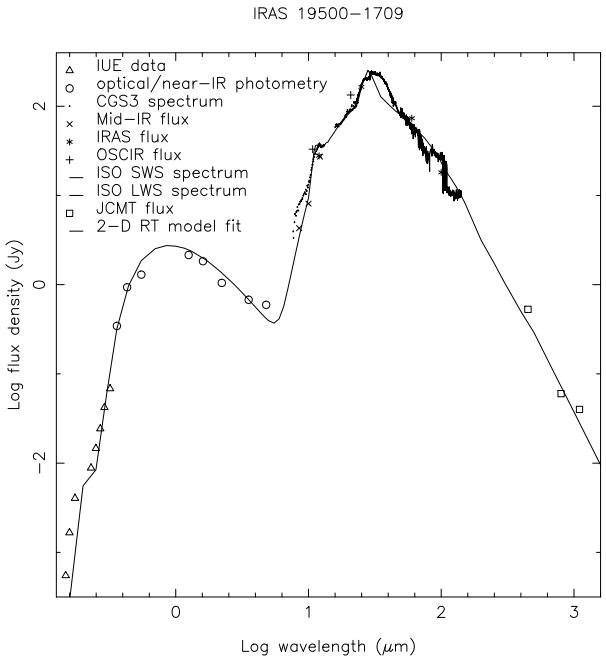

Figure 2. SED and model fit (solid black line).

a grain size power-law index of q=5. Reducing the value of q includes too many larger grains and so also results in a mid-IR peak which is too weak.

The fit to the 10-25 μm region is strongly affected by r_*/r_1 which determines the temperature of the warmest dust. A value of 8×10^{-5} provided the best fit. Increasing this value results in dust grains which are too hot and a poor fit around this region. Reducing the value of r_*/r_1 results in dust which is too cold and so not enough flux at mid-IR wavelengths and too much in the 40-160 μm region. The ratio of the inner shell radius to the outer shell radius (r_1/r_2) is determined to be 0.1 as this produces sufficient far-IR emission to fit the data longward of 100 μm. Extending the boundary any further than this produces too much far-IR emission.

After fitting the model to the data, the model curve was scaled to fit the observed flux. Table 2 shows the parameters for the model fit along with the derived parameters.

3.2 Derived parameters and the distance to 19500-1709

The profiles of the raw model images are double-peaked showing a resolved inner boundary. The inner boundary of the OSCIR images, however, is unresolved. In order to match the model to the data and so determine the scale of the model (i.e. the size of a model pixel in arcsec), the model images were smoothed using a Gaussian filter until they resembled the OSCIR images. Using smoothing steps of 1 model pixel, the Gaussian smoothing PSF was determined to have FWHM $>$ 11 pixels. A value less than this resulted in a dip in the profile so that FWHM=11 is the lowest value to show a single peak in the profile. Equating this degree of smoothing to the observed PSF (see Table 1) gives a model pixel size of 0.046 arcsec. This then leads to values of $r_1 < 0.4$ arcsec and $r_2 < 4$ arcsec (for $r_1/r_2 = 0.1$). Since $r_*/r_1 = 8 \times 10^{-5}$ then $r_* < 6.87$ R$_\odot$ and $L < 173$ L$_\odot$. These and other resulting upper limits on the derived parameters are listed in Table 2 for a distance of 1 kpc.

Schönberner (1983) determined lower limits for the mass and luminosity of central stars of PN of approximately 0.55 M$_\odot$ and 2500 L$_\odot$. If IRAS 19500-1709 is to be this luminous then it must be at a distance of at least 4 kpc. Pottasch & Parthasarathy (1988) conluded that $D = 5.5$ kpc based on the optical-IR energy balance. The value of r_*/r_1 is well constrained by the model fit: increasing or decreasing this value results in dust that is either too hot or too cool, respectively. We explored the possiblility that axisymmetric models might allow us to vary r_*/r_1, by redistributing the dust into a smaller volume of the shell, however the effect was minimal. Meixner et al. (1997) have used a larger value of $r_*/r_1 = 2.7 \times 10^{-4}$ but it is evident from their SED fit that the dust is too hot. With the model constraining r_*/r_1 in this way we conclude that IRAS 19500-1709 must be at least 4 kpc away for it to have the minimum luminosity consistent with a post-AGB status and this distance is adopted in the rest of the paper.

Dividing r_1 by the expansion velocity of the envelope (11 km s^{-1}, Likkel et al. 1987), shows that, for $D = 4$ kpc, the shell became detached (i.e. the high mass loss phase ended) at least 690 years ago. This is comparable to the result of 740 years obtained by Meixner et al. (1997). The age of the shell, calculated by dividing r_2 by the expansion velocity, is at least 6900 years.

The mass of dust in the shell and the grain number density at r_1 were calculated using an average of the densities of the 3 grain types used in the model and an average value for the extinction cross sections. Using the dust shell dimensions derived from the model fit, then to produce an extinction through the dust shell of $A_\mathrm{v} = 1.2$, which is needed to fit the SED, requires a dust number density at the inner shell radius of $n_1 = 5.6 \times 10^{-5}$ cm^{-3}, assuming $D = 4$ kpc. Using this number density, assuming a r^{-2} dust density distribution and an average grain bulk density of 2.56 g cm^{-3} results in a total mass of dust of $M_\mathrm{d} = 1.89 \times 10^{-3}$ M$_\odot$. Gledhill, Bains & Yates (2002) used their 850 μm SCUBA photometry to obtain a lower limit of $M_d > 1.6 \times 10^{-3}$ M$_\odot$ at 4 kpc.

Using a dust-to-gas mass ratio of 4.5×10^{-3}, an approximate value used for carbon-rich AGB stars (Jura 1986), the total envelope mass at $D = 4$ kpc is 0.42 M$_\odot$. According to our calculations the mass loss episode, responsible for the shell, lasted 6200 years so this results in an average mass loss rate of 6.8×10^{-5} M$_\odot$ yr^{-1} at this distance. This is comparable to the mass loss rate ($\dot{M}$) derived by Gürtler et al. (1996) of 6×10^{-5} M$_\odot$ yr^{-1} using a RT code and amC dust grains. It lies between the values derived by Meixner et al. (1997, $\dot{M} = 1.4 \times 10^{-4}$ M$_\odot$ yr^{-1}) and Hrivnak et al. (1989, $\dot{M} = 1.5 \times 10^{-5}$ M$_\odot$ yr^{-1}). Omont et al. (1993) calculate a value of $\dot{M} = 1.2 - 1.5 \times 10^{-5}$ M$_\odot$ yr^{-1} from CO line emissions. All of these rates are for $D = 4$ kpc.

Table 2. Model and derived parameters resulting from the final fit to the SED.

Parameter	Value
r_*/r_1	8x10^{-5}
r_1/r_2	0.1
A_v (mag)	1.2
q	5
a_{min} (μm)	0.01
a_{max} (μm)	2
T_{eff} (K)	8000
Grain type	
amC (%)	40
SiC (%)	30
MgS (%)	30
Grain temp. (min)	
amC (K)	53
SiC (K)	48
MgS (K)	42
Grain temp. (max)	
amC (K)	170
SiC (K)	155
MgS (K)	125
Derived parameters	
r_1 (cm/kpc)	$<$ 5.98x10^{15}
r_2 (cm/kpc)	$<$ 5.98x10^{16}
r_* ($R_\odot$/kpc)	$<$ 6.87
L ($L_\odot$/kpc^2)	$<$ 173
n_1 (cm^{-3}/kpc^{-1})	$>$ 2.2x10^{-4}
M_d ($M_\odot$/kpc^2)	$<$ 1.16x10^{-4}

3.3 Evidence for axisymmetry

Near-IR imaging polarimetry observations by Gledhill et al. (2001) show evidence for two scattering peaks on either side of the star, which suggest scattering from the inner edge of an axisymmetric envelope. The line joining the peaks is at PA$\sim$ 100°, approximately orthogonal to the elongation in the N band image of Fig. 1. The morphology appears remarkably similar to that described in mid-IR and near-IR imaging of 17436+5003 (Gledhill & Yates 2003; Gledhill et al. 2001). Although there is insufficient information in our OSCIR images to justify axisymmetric RT models, we suggest that 19500-1709 has an optically thin detached axisymmetric dust shell, resulting from enhanced equatorial mass-loss.

4 CONCLUSIONS

We present mid-infrared images and a model of the SED of IRAS 19500-1709 using amC, SiC and MgS grains. We find that small dust grains ($a_{min} = 0.01$ μm) and a steep power law size distribution (q=5) provide the best fit to the data. The observations constrain the inner radius of any detached dust shell to be a maximum size of 0.4 arcsec. Our results suggest that this object must be at a distance of at least 4 kpc to be sufficiently luminous to be a post-AGB star. We show that, at this distance, IRAS 19500-1709 would have an envelope mass of 0.42 $M_\odot$, that during the high mass-loss phase the mass-loss rate was 6.8×10^{-5} $M_\odot$ yr^{-1} and that this phase ended $\sim$ 700 yrs ago. Although the inner envelope structure has not been resolved in these OSCIR observations, there is evidence for axisymmetry along an axis perpendicular to that seen in near-IR imaging observations.

ACKNOWLEDGMENTS

This research has made use of the SIMBAD database, operated at CDS, Strasbourg, France. All model calculations were run on the HiPerSPACE Computing Facility at University College, London. We thank K. Justtanont for providing the UKIRT CGS3 spectrum. Scott Fisher is thanked for his help with the data. K. Clube is supported by a PPARC studentship.

REFERENCES

Begemann B., Dorscher J., Henning T., Mutschke H., Thamm E., 1994, ApJ, 423, L71
Draine B.T., Lee H.M., 1984, ApJ, 285, 89
Efstathiou A., Rowan-Robinson M., 1990, MNRAS, 245, 275
Gledhill T.M., Chrysostomou A., Hough J.H., Yates J.A., 2001, MNRAS, 322, 321
Gledhill T.M., Bains I., Yates J.A., 2002, MNRAS, 332, L55
Gledhill T.M., Yates J.A., 2003, MNRAS, 343, 880
Goebel J.H., Moseley S.H., 1985, ApJ, 290, L35
Gürtler J., Kömpe C., Henning Th., 1996, A&A, 305, 878
Hony S., Waters L.B.F.M., Tielens A.G.G.M., 2002, A&A, 390, 533
Hony S., Tielens A.G.G.M., Waters L.B.F.M., de Koter A., 2003, A&A, 402, 211
Hrivnak B.J., Kwok S., Volk K.M., 1989, ApJ, 346, 265
Jura M., 1986, ApJ, 303, 327
Justtanont K., Barlow M.J., Skinner C.J., Roche P.F., Aitken D.K., Smith C.H., 1996, A&A, 309, 612
Kwok S., Volk K., Bernath P., 2001, ApJ, 554, L87
Li A., Draine B.T., 2001, ApJ, 554, 778
Li A., 2003, ApJ, 599, L45
Likkel L., Omont A., Morris M., Forveille T., 1987, A&A, 173, L11
Likkel L., 1989, ApJ, 344, 350
Meixner M., Skinner C.J., Graham J.R., Keto E., Jernigan J.G., Arens J.F., 1997, ApJ, 482, 897
Omont A., Loup C., Forveille T., te Lintel Hekkert P., Habing H., Sivagnanam P., 1993, A&A, 267, 515
Parthasarathy M., Pottasch S.R., Wamsteker W., 1988, A&A, 203, 117
Pègouriè B., 1988, A&A, 194, 335
Pottasch S.R., Parthasarathy M., 1988, A&A, 192, 182
Schönberner D., 1983, ApJ, 272, 708
Speck A.K., Hofmeister A.M., 2004, ApJ, 600, 986
Speck A.K., Barlow M.J., Skinner C.J., 1997, MNRAS, 288, 431
Szczerba R., Omont A., Volk K., Cox P., Kwok S., 1997, A&A, 317, 859
Szczerba R., Henning Th., Volk K., Kwok S., Cox P., 1999, A&A, 345, L39
van der Veen W.E.C.J., Waters L.B.F.M., Trams N.R., Matthew H.E., 1994, A&A, 285, 551
van Winckel H., Reyniers M., 2000, A&A, 354, 135

van Winckel H., 2003, ARA&A, 41, 391
von Helden G., Tielens A.G.G.M., van Heijnsbergen D., Duncan M.A., Hony S., Waters L.B.F.M., Meijer G., 2000, Science, 288, 313

This paper has been typeset from a TEX/ LATEX file prepared by the author.